ECERS

Journal of the European Ceramic Society 20 (2000) 2591–2599

Nondestructive characterisation of alumina/silicon carbide nanocomposites using impedance spectroscopy

X. Wang, P. Xiao *

Department of Materials Engineering, Brunel University, Uxbridge UB8 3PH, UK

Received 16 December 1999; received in revised form 10 May 2000; accepted 14 May 2000

Abstract

Nondestructive evaluation (NDE) of ceramic matrix composites is essential for developing reliable ceramics for industrial applications. In the research described here, impedance spectroscopy has been used to characterise Al_2O_3/SiC nanocomposites nondestructively. Electrical modulus spectra from impedance measurements were used to determine the content of SiC nanoparticles in Al_2O_3/SiC composites. Meanwhile, electrical impedance measurements have been used to characterise the oxidation of Al_2O_3/SiC nanocomposites. Based on the microstructural features of the nanocomposites, equivalent models were developed to calculate the capacitance of the nanocomposites and oxidised specimens. The calculated results were used (i) to examine the relationship between the composition and electrical properties of the Al_2O_3/SiC nanocomposites; (ii) to predict the thickness of oxide scales formed at the surface of the nanocomposites after oxidation. The comparison showed reasonable agreements between theoretical prediction and experimental results. © 2000 Elsevier Science Ltd. All rights reserved.

Keywords: Al_2O_3–SiC; Composites; Impedance spectroscopy; Nondestructive evaluation; Oxidation

1. Introduction

Non-destructive evaluation is very important in both the manufacture and applications of ceramic materials. The brittleness, catastrophic failure behavior and low reliability of ceramics have been the main obstacles for the application of ceramics which lead to a high cost for ensuring the quality of ceramics by using expensive processing methods. Extensive studies have been carried out to investigate the processing and properties of advanced structural ceramics, which lead to not only significant improvements on the performance of ceramics, but also a better understanding of ceramic properties. However, much less has been done on non-destructive evaluation of ceramics, which is critical in controlling the quality of ceramics.[1] This is most likely due to the unavailability of an efficient and comprehensive NDE method that could be applied to the evaluation of ceramics. This research is to investigate the feasibility of using impedance spectroscopy as a non-destructive testing tool for evaluating structural ceramic materials.

A.C. impedance spectroscopy has been used to study electrolyte materials among which the best known is zirconia-based ceramics.[2] Impedance diagrams can be interpreted based on equivalent circuit models that can be related to microstructural features of the measured materials. In polycrystalline zirconia materials at a certain temperature, grains behave as ionic conductors, grain-boundaries and other microstructural defects, such as pores, cracks and any other second phases act as ionic blocking factors. In an impedance diagram (Nyquist plot) from measurements of zirconia ceramics, there are normally a high frequency (HF) semicircle which corresponds to the grains and a low frequency (LF) semicircle which corresponds to ionic blocking effects. Capacitance, resistance, relaxation frequency and depression angle can be obtained from the simulation of measured impedance diagrams. Such data can be used to characterise the microstructure of zirconia-based materials.[3–6] So far, extensive studies have been carried out to establish relationships between microstructural characteristics and electrical responses of ceramic materials.[2,7,8] Therefore, impedance spectroscopy is a potentially powerful technique for non-destructive evaluation of ceramic materials.

* Corresponding author. Fax: +44-1895-812-636.
E-mail address: ping.xiao@brunel.ac.uk (P. Xiao).

0955-2219/00/$ - see front matter © 2000 Elsevier Science Ltd. All rights reserved.
PII: S0955-2219(00)00134-5

Al_2O_3/SiC nanocomposites are attracting growing interest because significant improvements in strength and toughness have been achieved by the addition of SiC nanoparticles.[9,10] They are amongst the most promising structural materials that could be applied at high temperature up to 1000°C. Nondestructive evaluation of Al_2O_3/SiC composites is crucial for applications of this composite and other SiC containing ceramics. Studying oxidation of SiC containing ceramics at high temperature is also essential in application of these ceramics at high temperature. It was discovered that the oxidation rates of Al_2O_3/SiC nanocomposites are several orders of magnitudes higher than that of monolithic SiC.[11,12] Thus oxidation at high temperature could be a crucial factor in controlling the degradation of Al_2O_3/SiC nanocomposites at high temperature. It is highly desirable to develop a nondestructive evaluation technique for studying oxidation of Al_2O_3/SiC nanocomposites at high temperature.

In this study, impedance measurements have been used for the nondestructive evaluation of Al_2O_3/SiC nanocomposites. The modulus spectra were used to determine the content of SiC in Al_2O_3/SiC composites. The thickness of mullite/alumina layers resulted from the oxidation of Al_2O_3/SiC composites has been determined based on the impedance measurements and simulation of impedance diagrams. It has been proven that the impedance spectroscopy can be used (i) to examine the conducting mechanisms of ceramic materials, (ii) determine the content of conductive phase in insulating materials, (iii) determine the thickness of oxide scales formed at the surface of ceramic composites.

2. Experimental procedures

2.1. Sample preparation

As hot-pressed discs of Al_2O_3/SiC nanocomposites containing 5 vol.%, 10 vol.%, 20 vol.% SiC (denoted hereafter as 5SA, 10SA and 20SA, respectively), and monolithic alumina (hereafter denoted as MA) were obtained from the solid mechanics group at the Department of Materials, Oxford University. The detailed procedures for fabricating these materials were described in literature.[13,14] The composite discs were polished with 6 and 1 μm diamond paste for microstructural characterisation using both optical microscopy and scanning electron microscopy (SEM), coupled with energy dispersive spectroscopy (EDS).

2.2. The oxidation experiments

The samples were cut into a size of 10 mm×6 mm×2.2 mm from the as-processed discs. They were polished using 6 μm diamond paste and then cleaned in acetone before oxidation. Oxidation tests were conducted at a temperature between 800 and 1400°C in air for a period of 1–100 h. The heating and cooling rate were 3°C/min and 15°C/min, respectively. To measure the thickness of the oxide layer using optical microscopy, oxidized samples were cut using a precision diamond saw and polished using 6 μm diamond paste.

2.3. Impedance measurements

A Solartron SI 1255HF frequency response analyzer coupled with a 1296 dielectric Interface (Solartron, UK) was used for impedance measurements. Specimens for impedance measurement were in plate form, cut from discs. To examine the content of SiC in Al_2O_3 matrix, two parallel faces of the plates were ground, polished and cleaned before the application of silver or platinum electrodes. Silver or platinum pastes were painted on the surface as electrodes, then fired in air at 350°C for 15 min for the silver electrodes and at 1100°C for 1 h for the platinum electrodes. Oxidised specimens were examined without grinding and polishing. Conducting metal foils were applied directly to the surfaces of the specimens as electrodes. For impedance measurements at high temperature in a tube furnace, a metal tube connected to earth was used to shield the electromagnetic interference from the heating element in the tube furnace.

3. Results

3.1. Nyquist plots (Z' vs Z'')

There are at least two phases (SiC and Al_2O_3) present in the Al_2O_3/SiC nanocomposites, however, only one semicircle appears in the impedance spectra of the MA, 5SA and 10SA samples. This is because the relaxation frequency of SiC is well above the up frequency limit of the impedance analyzer (10^7 Hz in this case) and the resistivity of SiC is too low as compared to the Al_2O_3 matrix and other phases possibly present. However, Fig. 1 shows one large semicircle and one very small semicircle in the Nyquist plot of the 20SA sample after being exposed to a high temperature environment for sintering the platinum electrodes at 1100°C. To identify the effect of sintering the platinum electrodes, metal foils were applied as electrodes to the composite specimens with and without polishing after being exposed to air at 1100°C for 1 h. The impedance spectra showed there are two semicircles in the spectra for the oxidized specimens without polishing and one semicircle in the spectra for the specimen after polishing. These results indicate that the low frequency semicircle arises from the oxide scales on the surface of the 20SA specimens formed after sintering the platinum electrodes. However, for the 10SA

and 5SA samples, no second semicircle appeared in the spectra from R.T to 800°C. Fig. 2 shows the measured resistance of the 20SA sample, oxide scales from oxidation of the 20SA, and 5 SA samples as function of the reciprocal temperature. According to Fig. 2, the activation energy for electrical conduction across the 5SA sample is close to that across the oxide scales at the surface of the 20SA sample, which is also very close to that of alumina with purity 88%, but lower than that of alumina with purity 99.9% (the data for alumina with purity of 88 and 99.9% were from the literature).[15] The activation energy for conduction across the 20SA specimens is much lower than that of the 5SA specimens and the oxide scales. X-ray mapping of Si element in Al_2O_3/SiC nanocomposites displayed that SiC particles were clustered in the alumina matrix forming a network of SiC in 20SA specimens (Fig. 3). The conduction mechanism in the 20SA sample is very different from that in the 5SA samples and 10SA samples.

The extremely large resistance of the 5SA and 10SA specimens and oxide scales at the surface of the 20SA samples makes it difficult to measure the absolute value of the resistivity of these samples. The resistivity of 20SA at room temperature is in the range of 10^6–10^9 Ωcm. The resistivity of the 10SA was about two orders of magnitude higher than that of the 20SA at 400°C and the resistivity of MA was ten times higher than that of the 5SA at 600°C. Different measurements gave different values due to the electrode/specimen contact problem.

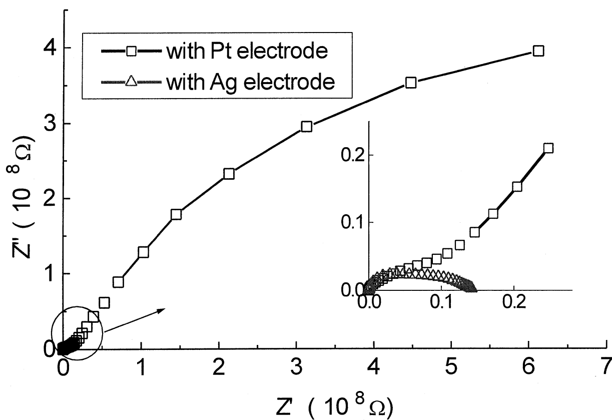

Fig. 1. The impedance spectra for 20SA specimens with fired platinum and silver electrodes at 300°C; the impedance spectrum obtained using silver electrode is referred to an enlarged diagram of the left bottom part of the spectra.

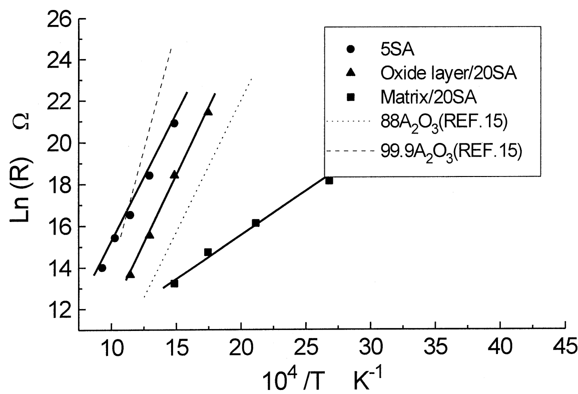

Fig. 2. Electrical resistance vs reciprocal temperature for 5SA, oxide layer and matrix of the 20SA specimen.

3.2. Modulus spectra

From impedance measurements, the electrical modulus (M) can be obtained, which is defined as:

$$M = j\omega C_e Z \tag{1}$$

where Z is the impedance, ω is the angular frequency, C_e is the capacitance of the empty cell and j is the imaginary unit.[16] Electrical modulus spectra can be obtained by plotting the modulus function in the complex plane.

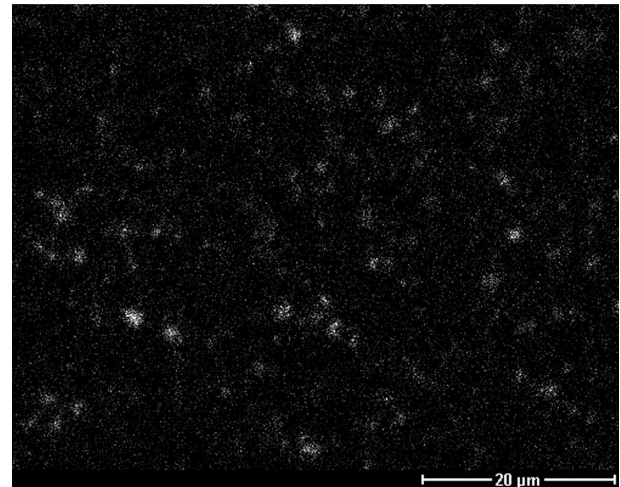

(a)

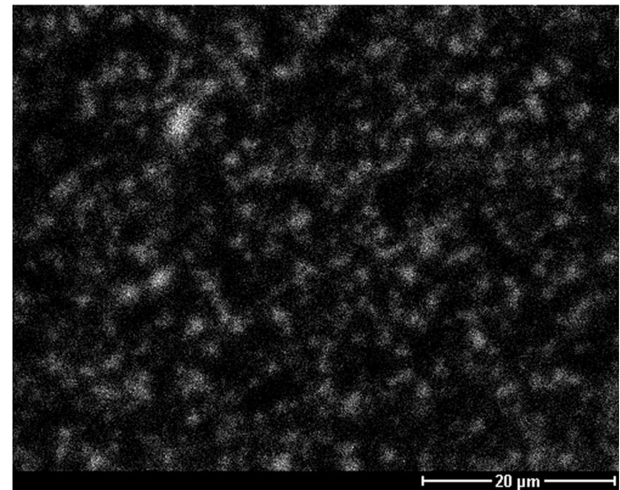

(b)

Fig. 3. X-ray mapping of SiC phase in (a), 5SA and (b) 20SA, where white spots represents the silicon content in alumina matrix.

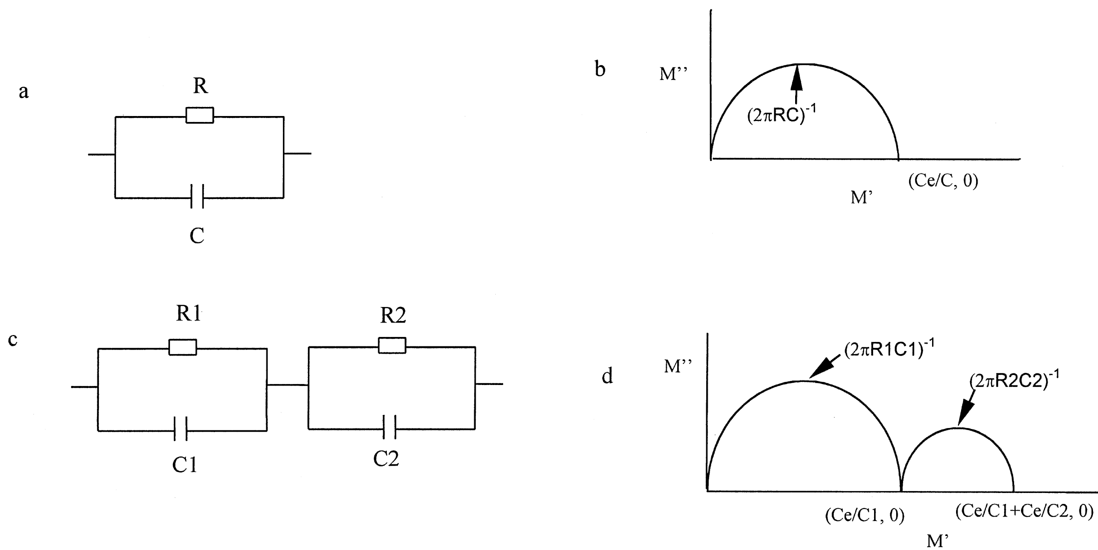

Fig. 4. Equivalent circuit models and corresponding modulus spectra, assuming $R_2^*C_2 < R_1^*C_1$.

For a simple circuit consisting of a resistor and a capacitor in parallel (a RC unit) as shown in Fig. 4a, the following formula can be derived from Eq. (1):

$$(M'')^2+\left(M'-\frac{C_e}{2C}\right)^2=\left(\frac{C_e}{2C}\right)^2 \quad (2)$$

This function represents a circle in the $M'-M''$ coordinate system with its center on the real axis $(C_e/2C,\ 0)$ and its diameter equal to C_e/C or $1/\varepsilon$ (Fig. 4b).

For a circuit with two RC units in series connection (Fig. 4c) the electrical modulus can be expressed as following:

$$M=M'+jM'' \quad (3)$$

Where

$$M'=\frac{\omega^2R_1^2C_1C_e}{1+\omega^2R_1^2C_1^2}+\frac{\omega^2R_2^2C_2C_e}{1+\omega^2R_2^2C_1^2} \quad (4)$$

$$M''=\frac{\omega R_1C_e}{1+\omega^2R_1^2C_1^2}+\frac{\omega R_2C_e}{1+\omega^2R_2^2C_2^2} \quad (5)$$

Calculations based on the above expressions show that whether or not two semicircles appear and how well the two semicircles are resolved depend on how different the resistance of R_1 is from R_2. When R_1 equals R_2, the modulus spectrum is shown in Fig. 5a, where two semicircles completely overlap. When R_1 is fifty times larger than R_2, two semicircular curves (Fig. 5b) can be identified, but not well separated. Two semicircles are well separated as shown in Fig. 5c when R_1 is three orders of magnitude larger than R_2.

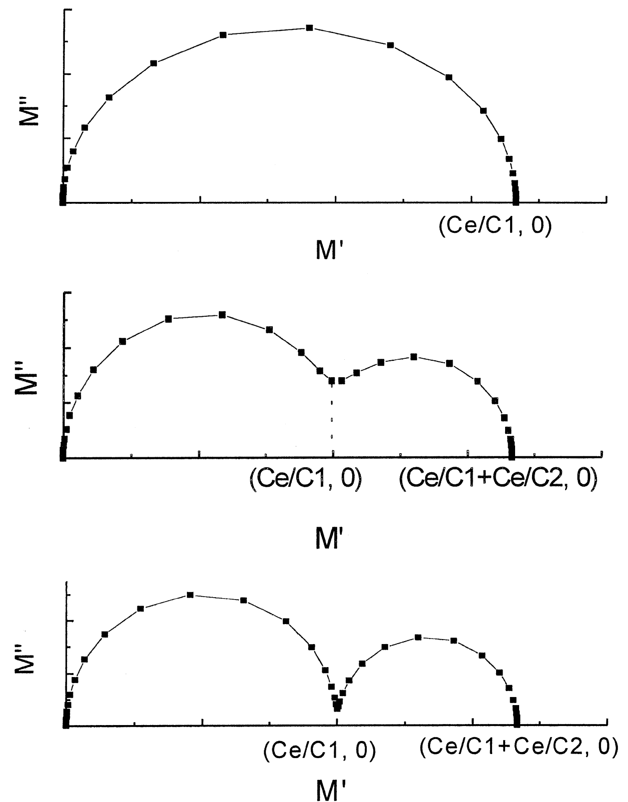

Fig. 5. Modulus spectrum for circuit model shown in Fig. 4b, (a), assuming $R_1 = R_2$; (b), assuming $R_1 = 1000^*R_2$;(c), assuming $R_1 = 1000^*R_2$.

Although there is considerable inconsistency in Nyquist plots of the 5SA, 10SA and 20SA specimens measured from time to time, modulus spectra of these specimens are consistent and stable. This indicates that the measurement of the dielectric properties of these specimens is much less affected by the contact problem between the electrode and specimen. Fig. 6 shows the

modulus spectra of the 20SA specimens at various temperatures. With an increase of temperature, the imaginary part of the modulus increases while the real part of the modulus decreases. Moreover, the relaxation frequency increases with an increase of temperature as well. However, it is still difficult to measure the dielectric property of 5SA and 10SA specimens due to high resistance of these specimens.

In order to obtain a stable current from materials with an extremely high resistivity for determining the dielectric properties of the 5SA and 10SA specimens, a new circuit was designed by connecting a 1 GΩ resistor in parallel with the measured specimens as shown in Fig. 7. The capacitance of the resistor (about 3–6 E^{-12} F) is less than 10% of that of the 5SA and 10SA specimens (–5 E^{-11} F) to be measured and the resistance of the resistor is much lower than that of the 5SA and 10SA specimens. The capacitive effect of this circuit is mainly contributed by the specimen while conduction mainly occurs across the resistor in parallel with specimens. The modulus spectra of this circuit (Fig. 8) show that all semicircles have a depressed part at the high frequency end. The conduction of the circuit (the imaginary part of the electrical modulus) arises from the conduction of the resistor at lower frequency and conduction from the specimen at high frequency. Measurements of 10SA specimens without being connected to the resistor generated spectra at high frequency as indicated in the amplified diagram in Fig. 8 (denoted a). No spectra could be obtained at lower frequency since the impedance at lower frequency is too high to be detected. The increasing conductivity of specimens results in the more depressed semicircles in modulus spectra.

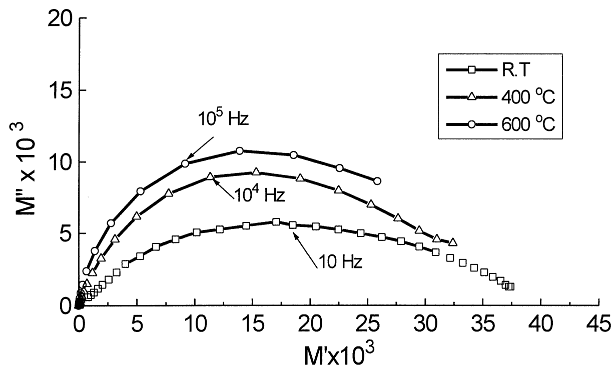

Fig. 6. Modulus spectra of 20SA at various temperatures.

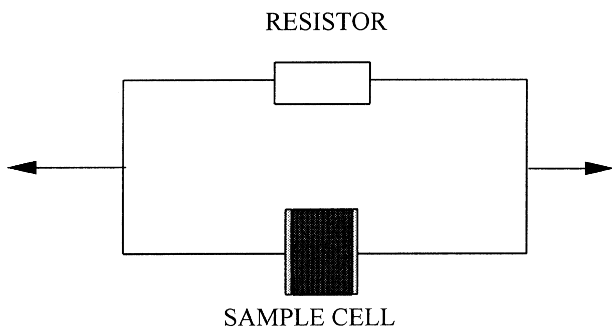

Fig. 7. A circuit with a resistor connected in parallel to the measured sample; the resistance of the resistor (R) is $1x10^9$ Ω, while its capacitance is about $2–4\times10^{-13}$ F.

Fig. 9 shows the dielectric constant obtained from measurements shown in Fig. 8, related to the content of SiC in the Al_2O_3 matrix. It clearly shows the data are reproducible with small errors with different experiments. The dielectric constant increases with increasing content of SiC in Al_2O_3. According to Fig. 9 the dielectric constant is 11.8 for pure Al_2O_3, which is a higher value than those (6–10.2) measured previously.[17] It should be noted that the edge effect on measurements was neglected here.

3.3. Modulus spectra of oxide scales formed from oxidation of 20SA specimens

Conducting metal foils were used as electrodes to study oxidation phenomena of 20SA specimens, which were exposed to air at temperatures from 800 to 1400°C

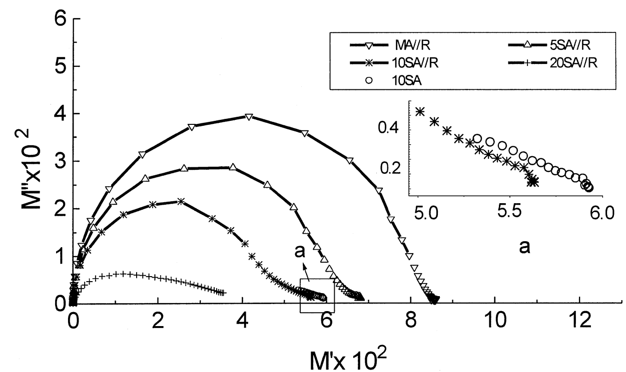

Fig. 8. Modulus spectra obtained at room temperature from measurements of the circuit shown in Fig. 7. with specimens containing different amounts of SiC.

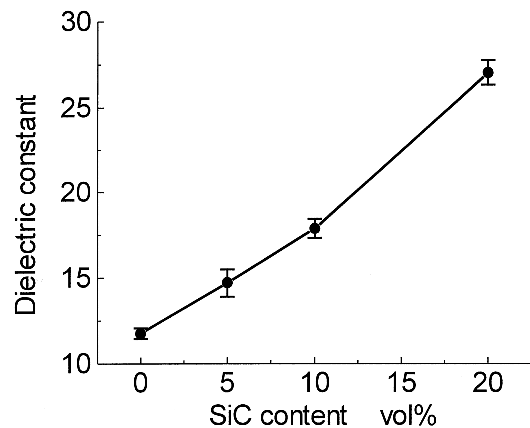

Fig. 9. Dielectric constant as a function of SiC content, where standard deviation is based on six sets of impedance measurements for each material.

for 1 h. Figs. 10 and 11 show the modulus spectra of two specimens from the oxidation of 20SA specimens for 1 h at 800°C and 1400°C, respectively. Although the impedance spectra of the specimen after oxidation at 800°C appear very similar in general shape to that of the sample without oxidation, close examination of the low frequency part of modulus spectra (Fig. 10b) finds a clear difference between the spectra from specimens before and after oxidation. In Fig. 11, the low frequency semicircle corresponds to a modulus spectrum of oxide scales formed after oxidation while a high frequency semicircle corresponds to modulus spectrum of bulk specimen. Table 1 gives a summary of semicircle diameters of both low frequency and high frequency for specimens oxidized at various temperatures, where we can see that the diameter of the low frequency semicircle increases with the increase of oxidation temperature, whereas the diameter of the high frequency semicircle is nearly constant. This indicates that little change occurs in the bulk specimens, but there is a gradual change of oxide scales formed at the surface of 20SA specimens.

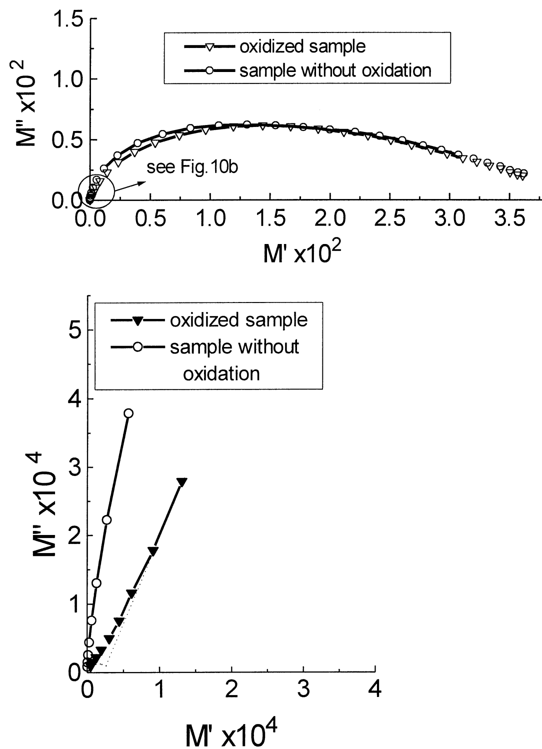

Fig. 10. (a) Modulus spectra 20SA specimens before and after oxidation at 800°C for 1 h; (b) the enlargement of diagram (a) at the left-bottom part.

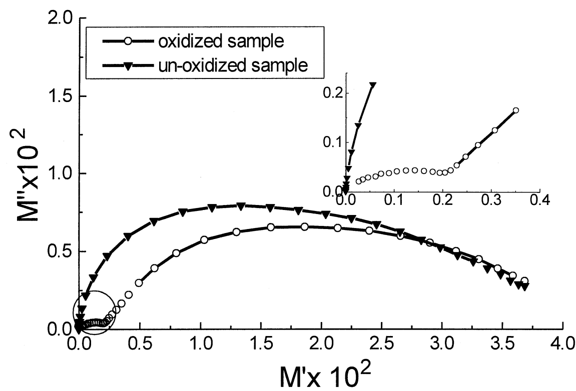

Fig. 11. Modulus spectrum for the 20SA specimen oxidized at 1400°C for 1 h.

4. Discussion

Experimental results showed there is a strong correlation between modulus spectra and the content of SiC in the Al_2O_3 matrix, which indicates that modulus spectroscopy can be used to determine the content of the conducting phase in an insulating matrix non-destructively. To simulate the dielectric property of the composites containing both conductive and insulating materials, the microstructure of the Al_2O_3/ SiC nano-composites is simplified as cubic units packing shown in Fig. 12a where SiC cubes are packed inside Al_2O_3 uniformly. The conductive SiC cubes behave as connection lines between capacitors with Al_2O_3 as the dielectric material. Where there is no SiC present along the electrical field direction, Al_2O_3 behaves as a capacitor with small area but large thickness. There is no edge effect being considered in this case. SiC cubes are assumed to be of uniform size inside the Al_2O_3. As the dielectric constant of Al_2O_3 was determined as 11.76 in Fig. 8, the dielectric constants of the composites can be calculated based on the model in Fig. 12 and these values are shown in Table 2. Apparently the predicted data are lower than the experimental data because this model is too simplified to give an accurate prediction of capacitance of the composites. Factors such as the irregular shape, non-uniform distribution of SiC particles and edge effect have not been taken account in this model, so further work is needed to predict the capacitance of the Al_2O_3/SiC composites accurately.

Previous research work on the oxidation of SiC/Al_2O_3 composites was carried out at temperature above 1300°C because it is difficult to use weight gain measurements or

Table 1
Semicircle diameters for 20SA oxidised for 1 h at various temperatures

Oxidation condition	LF semicircle diameter (D_{LF})	HF semicircle diameter (D_{HF})	D_{LF}/D_{HF}
800° C 1 h	2.5 x 10^{-5}	3.70 x 10^{-2}	6.75 x 10^{-4}
950°C 1 h	1.0 x 10^{-4}	3.69 x 10^{-2}	2.71 x 10^{-3}
1100°C 1 h	3.0 x 10^{-4}	3.66 x 10^{-2}	8.19 x 10^{-3}
1250°C 1 h	6.0 x 10^{-4}	3.60 x 10^{-2}	1.65 x 10^{-2}
1325°C 1 h	1.2 x 10^{-3}	3.58 x 10^{-2}	3.35 x 10^{-2}
1400°C 1 h	2.2 x 10^{-3}	3.48 x 10^{-2}	6.32 x 10^{-2}

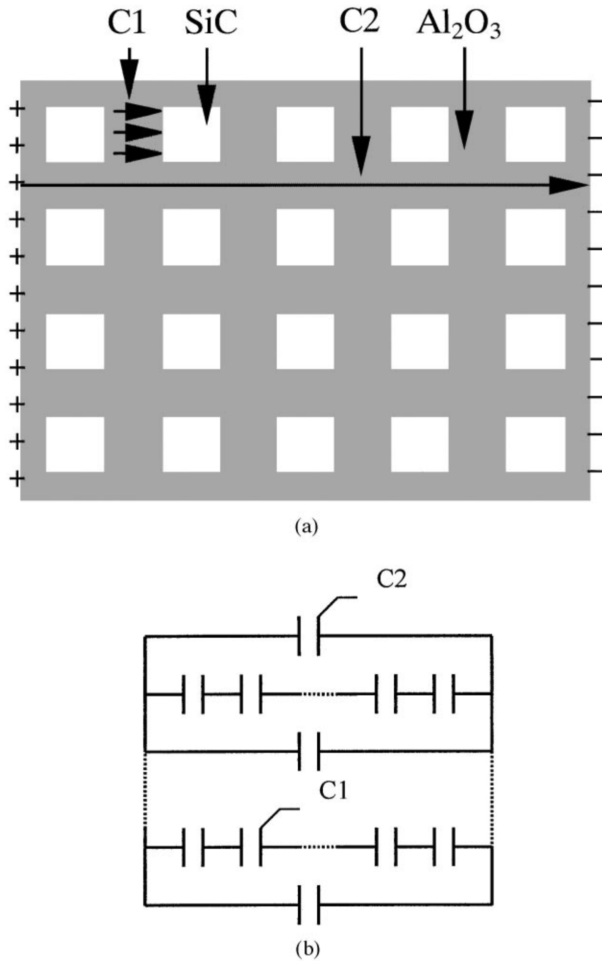

Fig. 12. (a), The idealized microstructure of the SiC/Al_2O_3 composites and (b), its equivalent circuit model.

Table 2
Dielectric constants of nanocomposites

Materials	Calculated ε	Measured ε
MA	11.76	11.76
5SA	12.69	14.7
10SA	13.95	17.86
20SA	17.42	27.03

electron microscopy for characterising the oxide scales formed at a lower temperature.[11,12] In the present study modulus spectroscopy was used to examine oxide scales formed at temperatures from 800 to 1400°C. The thickness of oxide scales can be predicted from the measurements of modulus spectra. For a sample of thickness t with an oxide layer of thickness δ at its surface (Fig. 13), the equivalent circuit model and ideal modulus spectrum of the sample should be similar to that shown in Fig. 4c and d. Here

$$C_1 = C_{ox} = \frac{\varepsilon_{ox}\varepsilon_o A}{2\delta} \tag{6}$$

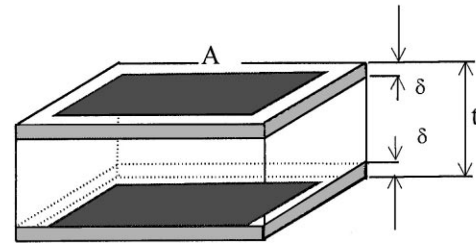

Fig. 13. $SiC–Al_2O_3$ composite of thickness t with an oxidation layer of thickness δ, 'A' representing the electrode area.

$$C_2 = C_{bk} = \frac{\varepsilon_{bk}\varepsilon_0 A}{t - 2\delta} \tag{7}$$

$$C_e = \frac{\varepsilon_0 A}{t} \tag{8}$$

C_1:capacitance of the oxide scale; C_2:capacitance of the bulk specimen without the oxide scale; C_e:capacitance of empty space occupied by the specimen.

Low frequency (LF) semicircle diameter

$$D_{LF} = C_e/C_{ox} = \frac{2\delta}{\varepsilon_{ox} t} \tag{9}$$

High frequency (HF) semicircle diameter

$$D_{HF} = C_e/C_{bk} = \frac{t - 2\delta}{\varepsilon_{bk} t} \tag{10}$$

The ratio of the LF semicircle diameter to HF semicircle diameter:

$$D_{LF}/D_{HF} = \frac{2\delta\varepsilon_{bk}}{\varepsilon_{ox}(t - 2\delta)} \tag{11}$$

Since the thickness of the oxide layer δ is much smaller than that of the sample t, the above formula can be written as:

$$D_{LF}/D_{HF} = \frac{2\delta\varepsilon_{bk}}{\varepsilon_{ox} t} \tag{12}$$

The thickness of oxide layer is calculated as

$$2\delta = \frac{\varepsilon_{ox} t}{\varepsilon_{bk}}(D_{LF}/D_{HF}) \tag{13}$$

Where t,ε_{ox} and ε_{bk} are constants for specimens with the same geometry and composition and values of D_{LF}/D_{HF} are listed in Table 1.

The dielectric constant of the 20SA sample was determined as 27.03 (Table 2). According to Eq. (13), ε_{ox} can be obtained if the thickness of the oxide scale is known. Fig. 15a shows the microstructure of oxide

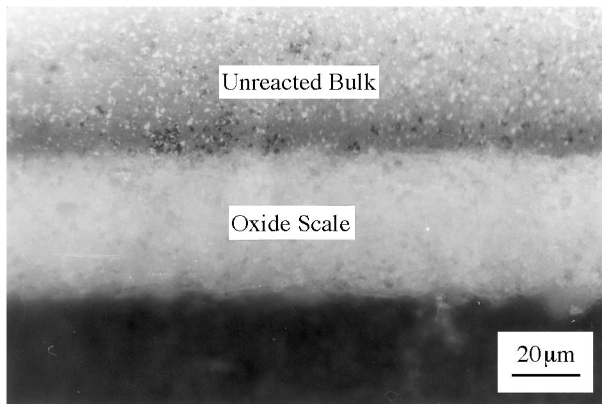

Fig. 14. Optical micrograph of cross-section of sample 20SA after oxidation at 1400°C for 64 h.

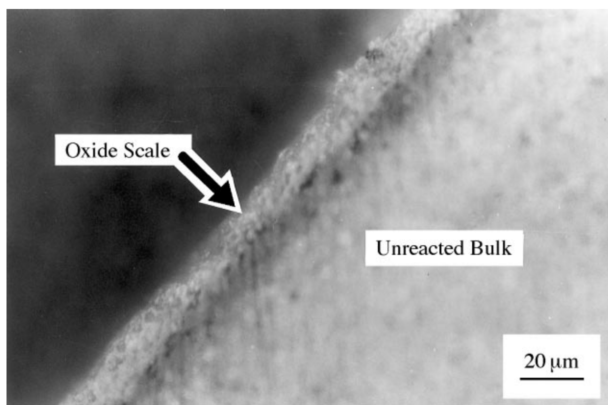

(a)

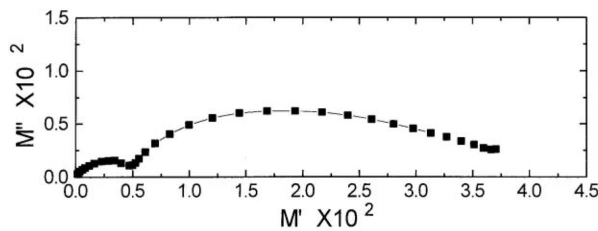

(b)

Fig. 15. (a) optical micrograph (b) modulus spectrum of the 20SA specimen after oxidation at 1400°C for 64 h, the oxide scale thickness being reduced to about 15 μm by polishing.

scales formed at the surface of the 20SA specimen where the bright phase layer is the mullite/alumina composite and the dark phase layer is mainly alumina. Both alumina and mullite have similar dielectric constants (6.2–16.8 for mullite and 6–10.2 for alumina).[17] Based on the modulus spectrum of this specimen (Fig. 15b) and Eq. (13), ε_{ox} was calculated as 3.5, which is lower than the dielectric constant of alumina or mullite. This could be due to the high porosity in the oxide scale (Fig. 14). The thickness of the oxide scales formed at different oxidation conditions was calculated based on $\varepsilon_{ox} = 3.5$ and $\varepsilon_{bk} = 27$ (Table 3). The thickness of the oxide scales is

Table 3
Calculated oxidation layer thickness at various temperatures

Oxidation condition	D_{LF}/D_{HF}	The calculated thickness
800°C 1 h	6.75×10^{-4}	0.15 μm
950°C 1 h	3.25×10^{-3}	0.59 μm
1100°C 1 h	8.19×10^{-3}	1.77 μm
1250°C 1 h	1.65×10^{-2}	3.58 μm
1325°C 1 h	3.35×10^{-2}	7.26 μm
1400°C 1 h	6.32×10^{-2}	13.70 μm

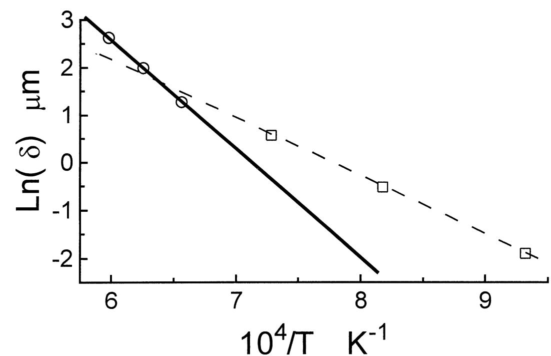

Fig. 16. Plot of the oxidation thickness δ against $1/T$, by linear regression, with the linear slope within the temperature range of 1250 to 1400°C equal to −2.276.

very difficult to measure using SEM due to the low contrast in the image between the oxide scale and the substrate. Meanwhile it is also very difficult to measure the thin oxide scale using optical microscopy. Therefore, impedance spectroscopy is the best tool for determining oxide growth of Al_2O_3/SiC nanocomposites.

Fig. 16 shows the plot of oxide scale thickness (δ) vs reciprocal of temperature. It appears that the activation energy at high temperature is higher than that at low temperature. The activation energy in the range of 1250–1400°C is calculated as 378 kJ/mol, which is closed to the previous results of 450–500 kJ/mol.[11,12] Therefore, it is promising to use impedance measurements for characterising kinetics on the oxidation of ceramics.

5. Conclusions

Impedance diagrams (Nyquist plots) of Al_2O_3/SiC nanocomposites show only one semicircle which corresponds to the impedance of Al_2O_3. The high conductivity and high relaxation frequency of SiC make it difficult to measure a semicircle corresponding to SiC. The electrical measurements indicated that conduction mechanisms of 5SA and 10SA specimens are similar to that of Al_2O_3 whereas the electrical conduction of the 20SA sample gets contribution from the network of SiC particles inside the composite. Moreover, the high electrical

resistance of the composites leads to poor reproducibility of impedance measurements.

Modulus spectra were used to determine the effect of SiC in the composites on dielectric properties of composites. A microstructural model was developed to calculate the dielectric properties of composites with insulating matrices and conductive inclusions. Oxidation kinetics was also examined using modulus spectroscopy. The activation energy was determined as 378 kJ/mol, which is close to previous results obtained using other methods. The oxide growth was predicted based on models developed for calculating capacitance of multi-layer structures. This study demonstrates that impedance spectroscopy is a useful technique for non-destructive evaluation of ceramic composites with insulating matrices and conductive inclusions.

Acknowledgements

We would like to acknowledge Mr. Houzheng Wu at Oxford University for providing the composite specimens and Professor B. Ralph and Dr. J. E. Shemilt at Brunel University for useful advice. We would also like to express our gratitude to Brunel University for financial support.

References

1. Van de Voorde, M. H., Non-destructive evaluation (NDE) of carbon-carbon (C-C) and ceramic composite material. *British Ceramic Transactions*, 1998, **97**(7), 287–292.
2. Dessemond, L., Muccillo, R., Henault, M. and Kleitz, M., Electrical conduction-blocking effects of voids and second phases in stabilized zirconia. *Appl. Phys.*, 1993, **A57**, 57–60.
3. Rodrigues, C. M. S., Labrincha, J. A. and Marques, F. M. B., Monitoring of the corrosion of YSZ by impedance spectroscopy. *J. Eur. Ceram. Soc.*, 1998, **18**, 95–104.
4. Muccillo, R., Muccillo, E. N. S. and Saito, N. H., Thermal shock behavior of ZrO_2:MgO solid electrolytes. *Mater. Let.*, 1998, **34**, 128–132.
5. Muccillo, E. N. S. and Kleitz, M., Impedance spectroscopy of Mg-partially stabilized zirconia and cubic phase decomposition. *J. Eur. Ceram. Soc.*, 1996, **16**, 453–465.
6. Steil, M. C., Thevenot, F. and Kleitz, M., Densification of ytria-stabilized zirconia-impedance spectroscopy analysis. *J. Electrochem. Soc.*, 1997, **1**, 390–398.
7. Smith, D. S., Lavielle, D. and Orange, G., Electrical response of microcracks in alumina/zirconia ceramic composites. *Silicates Industriels*, 1994, **5–6**, 165–167.
8. Santos, A. P., Domingues, R. Z. and Kleitz, M., Grain boundary segregation in high-purity, yttria-stabilized tetragonal zirconia polycrystals (Y-TZP). *J. Eur. Ceram. Soc.*, 1998, **18**, 1571–1578.
9. Niihara, K., New design concept of structure ceramic–ceramic nanocomposites. *J. Ceram. Soc. Jpn.*, 1991, **99**(10), 974–982.
10. Ohji, T., Hirano, T., Nakahira, N. and Niihara, K., Particle/matrix interface and its role in creep inhibition in alumina/silicon carbide nanocomposites. *J. Am. Ceram. Soc.*, 1996, **79**(1), 33–39.
11. Luthra, K. L. and Park, H. D., Oxidation of silicon carbide-reinforced oxide-matrix composites at to 1575°C. *J. Am. Ceram. Soc.*, 1990, **1375**, 1014–1022.
12. Sciti, D. and Bellosi, A., Oxidation behaviour of alumina–silicon carbide nanocomposites. *J. Mat. Sci.*, 1998, **33**, 3823–3830.
13. Sternitzke, M., Derby, B. and Brook, R. J., Alumina/silicon carbide nanocomposites by hybrid polymer/powder processing microstructures and mechanical properties. *J. Am. Ceram. Soc.*, 1998, **81**(1), 41–48.
14. Wu, H. Z., Lawrence, C. W., Roberts, S. G. and Derby, B., The strength of Al_2O_3/SiC nanocomposites after grinding and annealing. *Acta Mater.*, 1998, **11**, 3839–3848.
15. Moulson, A. J. and Herbert, J. M., *Electroceramics*. Chapman & Hall, London, 1995, p. 215.
16. Macdonald, R., *Impedance Spectroscopy*. John Wiley & Sons, New York, 1987, p. 7.
17. Buchanan, R. C., *Ceramic Materials for Electronics*. Marcel Dekker, New York, Basel, 1991, p. 4.